Proceedings of the 34th Chinese Control Conference
July 28-30, 2015, Hangzhou, China

Expansion Rate based Collision Avoidance for Unmanned Aerial Vehicles

LEI Xin, WANG Xiangke, LI Jie, ZHANG Guozhong, SHEN Lincheng

Department of Mechatronics and Automation, National University of Defense Technology, Hunan 410073
E-mail: lei_xx@126.com

Abstract: Collision avoidance is a critical problem for Unmanned Aerial Vehicles (UAVs) for its wide application. We proposed a vision based collision avoidance approach for UAVs, based on potential field method. By exploring human navigation model, the potential field is designed over the UAV's heading using the relative heading to the goal and to obstacles, the distance to the goal, and the expansion rate of obstacles. This method is independent of any information of obstacles, and controls the UAVs heading directly away from the obstacle and towards the goal. The simulation results show that the paths are smooth and much more optimal and robust compared with the model with angular width.

Key Words: Collision avoidance, Human navigation model, Expansion rate, Potential field

1 Introduction

Collision avoidance is a critical problem to be solved for Unmanned Aerial Vehicles (UAVs) for its wide applications. With the limitation of the detection capability, many collision avoidance strategies based on the accurate localization information become unavailable, such as geometry methods [1], optimization theory [2], and artificial intelligent algorithms [3].

For small UAVs, constrained by the payload capability, small, weightless, and powerless visual detectors become a natural choice. Vision based collision avoidance researches for UAVs is a kind of non-cooperative approach, mainly including two classes of work, one is object and collision detection [4], [5], [6], the other is collision avoidance strategy [7], [8]. On one hand, the objects can be detected up to the distance of more than 3 miles [5], and the time to collision can be extracted directly through the expansion segmentation method without target identification [6], which is used to detect the collision but is time-consuming. On the other hand, most of the non-cooperative collision avoidance strategies adopt the state estimation methods, without accounting for the visual information.

However, for fast moving UAVs, there is not much time to carry out the complicated algorithms. For this sake, the reactive collision avoidance method becomes a natural choice. There are several researches on this topic. Taking inspiration from neural and behavioral strategies of flying insects, Antoine Beyeler et al. [9] cast optic flow measurements into control signals, proposing a simple mapping directly from sensing to acting. However, this method requires distinct optic flow information, which usually comes from large obstacles, like buildings and trees. Aaron Mcfadyen [10], [11] uses angular measurements directly as feedback in the framework of visual servoing control, which is consistent with human visual navigation behavior in a collision scenario, without relying on range. They design a controller to track the spiral curve [12], which leads the quadrotor to spiral around the obstacle and resume a normal flight when it passes the obstacle. However, for UAVs, the spiraling action is not generally accepted in normal flight. Wesley H. Huang et al. [13] presents an obstacle avoidance approach using a single camera without recovering depth. Their method is based on Fajen and Warren's model of human navigation [14], [15], [16]. They formulate the navigation model as a potential field model and take into account the angular width of an obstacle to prevent the potential collision. Because it controls the angular acceleration, it is directly applicable to steering the nonholonomic vehicles. The prior information about the minimum obstacle's size needs to be known, which may not be obtained in many practical situations.

In this paper, we propose a collision avoidance approach using the visual cue of expansion rate, inspired by human navigation model [14], [15]. We make use of the real-time performance of the potential field method, casting the expansion rate into the potential function to realize a reactive avoiding behavior. The potential field method has been widely used in obstacle avoidance problem for robot since early time. It was first developed by Khatib in 1986 to make better use of low level control capabilities in performing real-time operations [17], which provides the foundation for reactive collision avoidance. We compute a potential field with the relative headings to the goal and to obstacles, the distance to the goal, and the expansion rate of the obstacle. The UAV is then controlled by an angular acceleration. The advantage of this approach is that it is no need to know any information about the obstacle, which may much more suitable for the non-cooperative situations. Compared with the method using angular width, the performance is much more optimal. Besides, as the information about the obstacle is not necessary, this approach is more robust to the inaccuracy of the estimation.

The paper is organized as follows. We describe the problem in section 2. In section 3 we explain the proposed approach. Simulation results are provided in section 4. Lastly, section 5 presents conclusions.

*This work is supported by National Natural Science Foundation (NNSF) of China under Grant 61403410.

2 Problem Descriptions

2.1 Dynamics

We consider a 2-dimensional movement for UAVs, with constant altitude and airspeed (v) by the control of the longitudinal dynamics [18]. The following is a simple kinematic model that will be used to study the collision avoidance behavior of the proposed approach and generate a set of new positions:

$$\begin{cases} \dot{x} = v\cos\psi \\ \dot{y} = v\sin\psi \end{cases} \tag{1}$$

where heading ψ will be controlled by the potential field collision avoidance model presented in next section.

Starting from the simplicity, we consider the static obstacle scenarios, in which obstacles are assumed to be circle with various radii of r_{oi}, located at the position of (x_{oi}, y_{oi}).

Local sensing information is obtained through a spherical camera model fixed on UAVs. Spherical cameras provide a 4π steradian field of view [11], such that we do not need to deal with the problem of obstacles running out of the field of view. There is an analytical form of spherical projection of a sphere [19], but we here consider a simplified one, which is:

$$\theta = 2 * \arcsin(d_o / r_o) \tag{2}$$

where θ is the angular width of the image feature, and d_o is the distance between obstacles and vehicles. Assuming the camera is held steady by a cloudy platform, and the optical axis is aligned to the body axis, the information one can obtain from the single camera will be the heading to the obstacle ($\psi - \psi_o$) and the obstacle's angular width, shown as Fig.1.

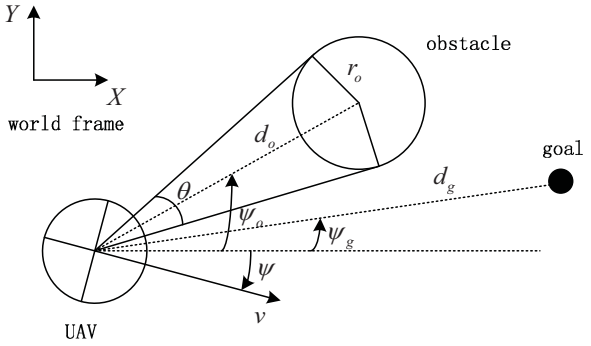

Fig. 1: ψ , ψ_g , ψ_o are respectively the heading of the UAV, the goal and an obstacle to the world X axis. Distance to the goal d_g and the obstacle d_o, the size of the obstacle r_o and the angular width θ are also shown.

As UAVs approaching to an obstacle, the image feature expands with the rate of $\dot{\theta}$, a differential of the angular width with time. We use the expansion rate to design a potential function in section 3.

Assume that the goal heading and distance are known. For UAVs, the goal may be a preplanned waypoint stored in the autopilot.

2.2 Human Navigation Model

The basis of this approach is the acceleration model devised by Fajen and Warren [15] from experiments on human walking performed in a virtual environment, interpreted as a function of the heading angle:

$$\begin{aligned} \ddot{\psi} = &-b\dot{\psi} - k_g(\psi - \psi_g)(e^{-c_1 d_g} + c_2) \\ &+ \sum_i k_{oi}(\psi - \psi_{oi}) e^{-c_3|\psi - \psi_{oi}|} e^{-c_4 d_{oi}} \end{aligned} \tag{3}$$

which includes three terms: a damping term, a goal term, and an obstacle term. It shows that the angular acceleration toward the goal increased with goal angle and decreased exponentially with goal distance, while angular acceleration away from the obstacle decreased with both obstacle angle and distance.

For simplicity, the damping term was assumed to be proportional to turning rate, with proportion being some constant $b > 0$.

The goal term behaves as an attractor, pulling the robot towards it. The parameter k_g determines the strength of the goal term, c_1 modulates the rate of exponential decay with goal distance, and c_2 sets the minima acceleration toward the distant goal.

Meanwhile, the obstacle term behaves as a repellor, pushing the robot away from it. The parameter k_o determines the strength of the obstacle term, c_3 scales the rate of decay with obstacle angle, and c_4 adjusts the rate of decay with obstacle distance.

2.3 Tasks

Based on the framework described above, the task is then to generate a control law to lead the UAV successfully avoid obstacles and reach the goal in any given scenarios. Specifically, three configurations will be considered, which are 1) a single obstacle, 2) two obstacles, and 3) an obstacle with inaccurate size estimation.

The objective is to prove that the model defined with expansion rate is able to generate a smooth and reasonable path. Meanwhile, since it is independent of size information of the obstacle, it will be robust to the estimation error. Compared with the model defined with angular width, it is expected that the performance is much better.

3 Methodology

In human navigation model, the goal term behaves as an attractor, pulling the robot to close the heading angular gap and distance gap, while the obstacle term behave as a repellor, pushing the robot to increase the heading angular gap and distance gap. It is just like the robot is in a potential field. Different from the original potential field method, the robot here is controlled by an angular acceleration rather than the virtual forces. In the original potential field method, the potential function is derived by taking the negative integration to the position. Similarly, when taking the negative integration to the robot's heading for the human navigation model, we obtained the potential field function defined over the heading angular, which will attract the agent's heading close the angular gap to the goal, and repel it away from the angular gap to the obstacle.

Based on that, to remove the dependence of the distance to the obstacle, which is hard to be obtained with mono-visual camera, we replace the distance term in the obstacle term with expansion rate, properly magnified. It is believed that the expansion rate represents information about the relative movement, and predicts collisions. As such, we cast the expansion rate into the potential field function, resulting in our method of collision avoidance with expansion rate, which will be described in 3.2.

To compare with the method using angular width [13], we briefly describe the method in 3.3.

3.1 Potential Field Model

The acceleration model can be interpreted as a potential field where the goal and obstacles give rise to potential functions over the agent heading [13]. The agent is then controlled according to:

$$\ddot{\psi} = -\frac{d\Phi}{d\psi} - b\dot{\psi} \tag{4}$$

where Φ is the overall potential, consisting of goal potential Φ_g and obstacle potential Φ_o, respectively expressed as:

$$\Phi_g[\psi_g, d_g](\psi) = \frac{1}{2} k_g (\psi - \psi_g)^2 (e^{-c_1 d_g} + c_2) \tag{5}$$

$$\Phi_{oi}[\psi_{oi}, d_{oi}](\psi) = k_o \frac{c_3 |\psi - \psi_o| + 1}{c_3^2} e^{-c_3|\psi-\psi_{oi}|} e^{-c_4 d_{oi}} \tag{6}$$

which can be obtained by taking the negative integration with respect to ψ of the goal and obstacle components of Eq. (3), respectively. The potential landscape keeps changing as the robot moves, since the heading to the obstacles and the goal is in the state of changing.

3.2 Potential Field Model using Expansion Rate

The expansion rate of the obstacle reflected in the image can be related with the distance, size, and relative velocity of the obstacle [20]. There might be some predictive timing information involved in it, which though has not been explicitly explained. With no requirement of the prior information about the obstacle, the expansion rate is used to replace the distance term $e^{-c_4 d_{oi}}$ in Eq. (6). As the expansion rate is not big enough to play a part in the potential function, a magnification factor is multiplied to it. In practice, this can be achieved by making use of a long focal length camera. The obstacle potential is then as:

$$\Phi_{oi}[\psi_{oi}, \theta_i](\psi) = k_o \frac{c_3 |\psi - \psi_{oi}| + 1}{c_3^2} \bullet e^{-c_3|\psi-\psi_{oi}|} k_e \dot{\theta}_i \tag{7}$$

where $\dot{\theta}_i$ is the expansion rate of the i th obstacle, k_e is magnification factor for the expansion rate. This form of obstacle potential function increases proportionally as obstacles approaching and decreases exponentially with the bearing of obstacles.

3.3 Potential Field Model using Angular Width

Out of the considerations that [13]: 1) wider obstacles generate a wider obstacle potential, 2) the potential approach infinity as the robot gets closer and closer to the obstacle, and 3) remove the dependence on the distance to obstacles, the tangent function was chosen to drive the potential toward infinity as the angular width θ_i increases to some maximum value. The obstacle potential function defined by angular width is then as [13]:

$$\Phi_{oi}[\psi_{oi}, \theta_i](\psi) = k_o \frac{c_3 |\psi - \psi_{oi}| + 1}{c_3^2} e^{-c_3|\psi-\psi_{oi}|} \bullet (\tan(\theta_i + c_5) - \tan c_5) \tag{7}$$

where the term $e^{-c_4 d_o}$ is replaced by $(\tan(\theta_i + c_5) - \tan c_5)$ where θ_i is the angular width of the i th obstacle and c_5 is a new parameter defined as:

$$c_5 = \frac{\pi}{2} - 2\tan^{-1}\left(\frac{r_o}{r_o + r_r}\right) \tag{8}$$

where r_o is the obstacle radius and r_r is the robot radius.

Noted that, c_5 is conservatively set using the radius of the smallest obstacle. This is a trade-off with obstacle distance, which will make the robot avoid distant large obstacles conservatively, i.e. go further around the obstacles.

4 Simulations and Results

To analyze the performance of the devised method in section 3, numerical simulations are conducted. Simulation scenarios are set as follows. A small UAV is flying at a constant altitude. The point mass UAV model described in section 2 is adopted. The heading of the UAV is in the east direction, pointing at the goal, which is one of the waypoints ahead. Obstacles are set at the location between the start point and the goal. The UAV starts from a proper position, within which the obstacles are able to be detected by the camera model. To demonstrate the proposed method, we set three configurations: 1) one single obstacle; 2) two obstacles; 3) an obstacle with inaccurate size estimation.

4.1 Simulation Preparation

Refer to [13], the model parameters used in the simulation is provided as Table 1. Table 2 summarizes the parameters used in the simulations.

Table 1: Model parameters

Damping coefficient	$b = 5.5$
Strength of the goal term	$k_g = 2.0$
Decay rate with goal distance	$c_1 = 0.4$
Minima acceleration toward the goal	$c_2 = 0.4$
Strength of the obstacle term	$k_o = 9.0$
Decay rate with obstacle angle	$c_3 = 3.0$
Decay rate with obstacle distance	$c_4 = 0.025$

Table 2: Parameters used in simulations

Sensing range	$R_{\text{detect}} = 1500m$
Size of UAV	$r_{UAV} = 5m$
Safety radius of UAV	$r_{safe} = 15m$
Size of obstacle 1	$r_{obs1} = 20m$

Size of obstacle 2	$r_{obs2} = 10m$
Relative velocity	$V_r = 0.9m/s$
Starting point	$P_{start} = (0,0)$
Goal position	$P_{goal} = (1000,0)$
Magnification factor	$k_e = 200$

4.2 Scenario 1: one single obstacle

In the first scenario, we set one obstacle in the location of (500, 0.5) far from the aircraft initial position, with a little bit of bias from the line aligned the start point to the goal position, such that the initial potential won't be zero. Fig.2 (a) shows that the UAV is able to avoid the obstacle, performing a natural and effective maneuver. The magenta colored line represents collision avoidance path generated by the potential field model with expansion rate. The red circle represents the obstacle with a radius of 20 m. The green circle represents the UAV with a safety zone. The number beside it illustrates the minimum distance between the UAV and the obstacle, which is about 74.1 m. A good performance is evidenced, showing the feasibility of the proposed model.

Fig.1 (b) shows the change of the heading angle and the expansion rate when the UAV carries out the avoiding maneuver. The maximum heading is about 15 degree. When the UAV turns to the goal, it flies to the goal directly, in the direction of fasted decrease the potential. The expansion rate, curve presents a symmetry about the location where the distance between the obstacle and the UAV reaches the minimum.

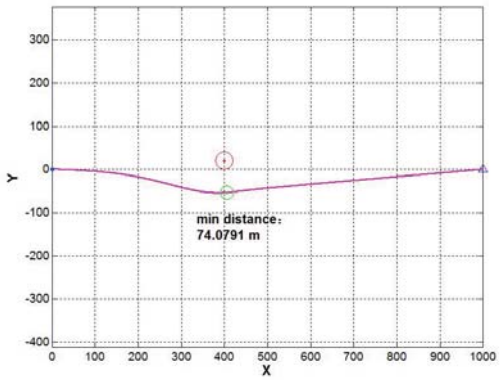

(a)

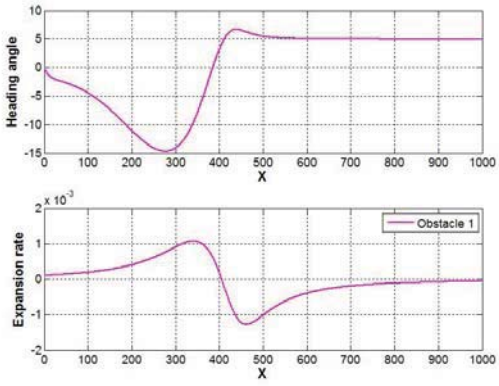

(b)

Fig. 2: Successfully avoid a single obstacle. (a) avoiding path; (b) upper: heading angle; below: expansion rate.

4.3 Scenario 2: two obstacles

In this scenario, two obstacles are located at (400, 20) and (600, -55). Assume that there is no sheltering of each other for the two obstacles. Fig.2 (a) illustrates the UAV takes a smooth and reasonable path through the two obstacles, where the minimum distance away from the two obstacles are respectively 76.8 m and 52.3 m. The heading angle shown in Fig.2 (b) is not as smooth as participate, but can also be acceptable. As shown in Fig.2 (b), the angular width expands much more quickly when the UAV encounters the smaller and distance obstacle.

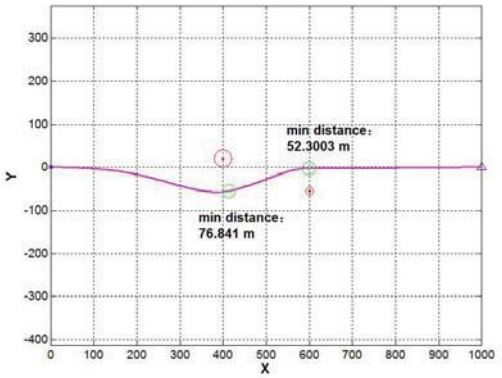

(a)

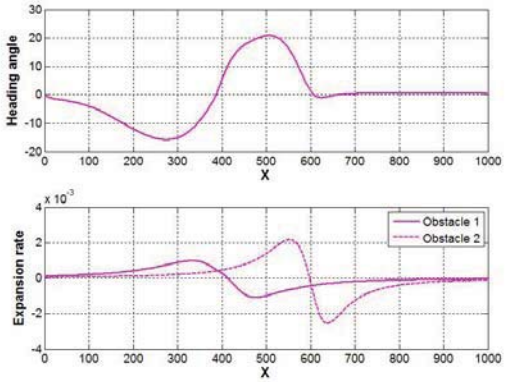

(b)

Fig. 3: Take a reasonable, smooth and natural path through two obstacles. (a) avoiding path; (b) upper: heading angle; below: expansion rate.

4.4 Scenario 3: an obstacle with inaccurate size estimation

In the third scenario, we consider an obstacle located at (500, 0.5), and with its actual size of 20 m (red colored circle) while the estimated size 5 m (green colored circle). Fig.4 (a) shows that there is no impact for the avoiding performance, i.e. the result is the same as the one in scenario 1. This is because with expansion rate, there is no need to know the accurate size of the obstacle, and the UAV just avoids the obstacle according to what it "sees".

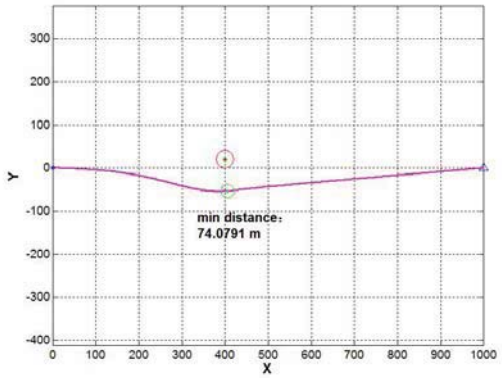

(a)

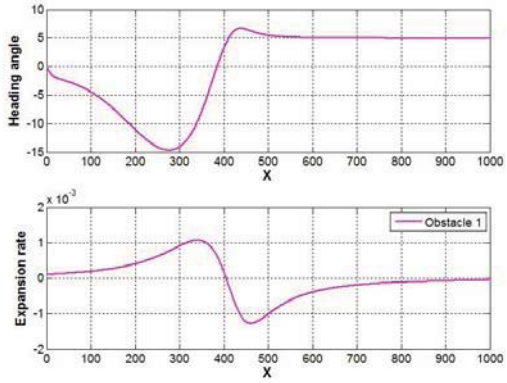

(b)

Fig. 4: Avoid an obstacle with size estimation error. (a) avoiding path; (b) upper: heading angle; below: expansion rate.

4.5 Comparison with the potential model using angular width

In this section, we compare the model using expansion rate with the one using angular width. We set the same three scenarios as 4.2, 4.3 and 4.4. Our purpose is to demonstrate that the expansion rate model is feasible, optimal and robust to the error. The results are respectively shown in Fig.5, Fig.6 and Fig.7.

As seen in Fig.5 (a), the UAV avoid the obstacle with much more deviations from the preplanned path, the minimum distance away from the obstacle is 95.2 m, which is farther away than the results of the model with expansion rate.

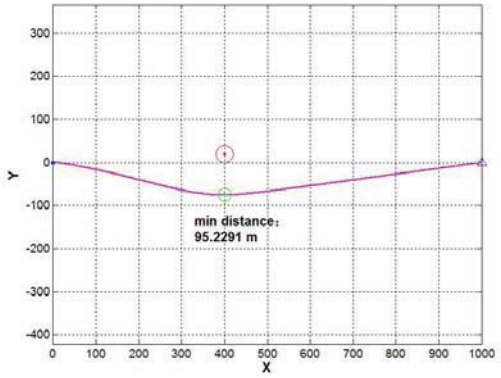

(a)

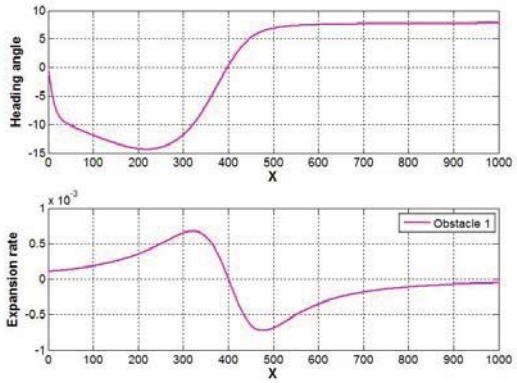

(b)

Fig. 5: Avoid one single obstacle with more deviation from the preplanned path than expansion rate. (a) avoiding path; (b) upper: heading angle; below: expansion rate.

Fig.6 shows that the UAV takes a conservative path around the obstacles. Because it uses the minimum obstacle's size, the UAV regards the first large obstacle as a small one located much nearer. As a result, the UAV starts the avoiding behavior earlier and take a path farther away from the obstacle. When it passes the large obstacle, for the constraint of the maneuver capability, the UAV cannot pass the second obstacle through the space between the two obstacles. Obviously, the path cost is more than the one of expansion rate.

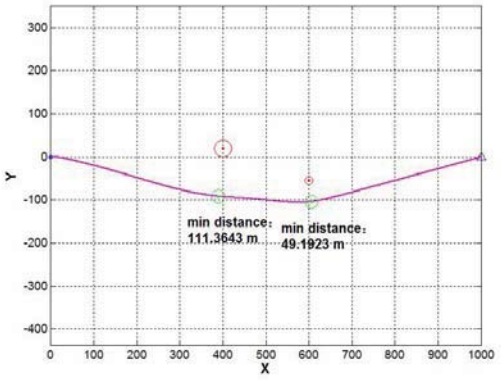

(a)

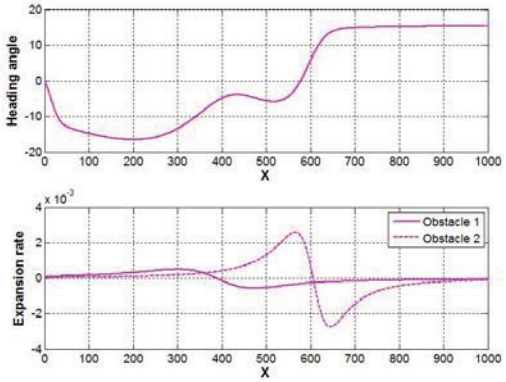

(b)

Fig. 6: Avoid two obstacles in a conservative way. (a) avoiding path; (b) upper: heading angle; below: expansion rate.

Fig.7 (b) presents a result under the inaccurate estimation of the obstacle's size. It shows that the minimum distance

between the UAV and the obstacle is 112.3 m, much more than the one of expansion rate, which means the UAV takes a long way around the obstacle.

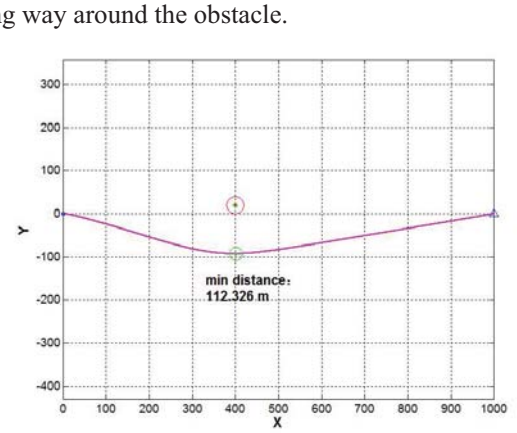

(a)

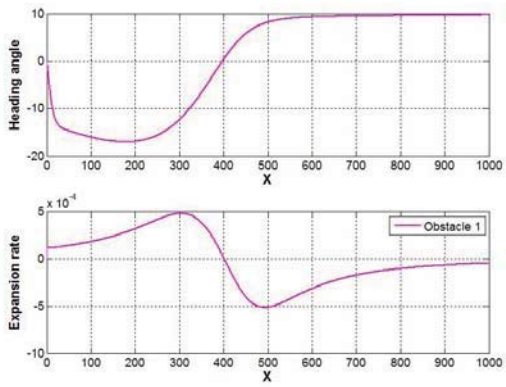

(b)

Fig. 7: Avoid an obstacle with estimation error. (a) avoiding path; (b) upper: heading angle; below: expansion rate.

5 Conclusions

In this paper, we proposed a collision avoidance approach using expansion rate, based on the model of human local navigation. We casted the expansion rate into potential field function to realize the reactive avoiding behavior. A spherical camera model was adopted to ensure the visibility throughout the encounter. The potential field model is defined over the UAVs' heading, which can control the nonholonomic vehicles directly. We use the angles to the obstacle and the goal, the distance to the goal, and the expansion rate of the obstacle to compute the potential field. Independent of the information of the obstacle, it is suitable to non-cooperative situations. Simulation results demonstrate that the paths are smooth and have a continuous curvature, which means our method is effective. Compared with the model with angular width, our model is much more optimal and robust to the inaccuracy of the size information.

References

[1] C. Carbone, U. Ciniglio, F. Corraro, and S. Luongo, A novel 3D geometric algorithm for aircraft autonomous collision avoidance, in *Proceedings of 45th IEEE Conference on Decision and Control*, 2006: 1580–1585.

[2] H. B. Duan, G. J. Ma, D. B. Wang, and S. Q. Liu, An improved antcolony algorithm for solving continuous space optimization problems, *J. Syst. Simul.*, 2007, 19(1): 974–977.

[3] G. B. Lamont, J. N. Slear, and K. Melendez, UAV swarm mission planning and routing using multi-objective evolutionary algorithms, in *Proceedings of Computational Intelligence in Multicriteria Decision Making*, 2007: 10–20.

[4] L. John, J. F. Jason, M. Luis, and O. S. Peter, Characterization of Sky-region Morphological-temporal Airborne Collision Detection, *Journal of Field Robotics*, 2013, 30(2): 171-193.

[5] L. John, M. Luis, and J. F. Jason, Airborne Vision-Based Collision-Detection System, *Journal of Field Robotics*, 2011, 28(2): 137-157.

[6] B. Jeffrey, J. T. Camillo, Expansion Segmentation for Visual Collision Detection and Estimation, in *Proceedings of IEEE International Conference on Robotics and Automation*, 2009: 875–882.

[7] Y. Xilin, M. A. Lius, and B. Troy, A 3D Collision Avoidance Strategy for UAVs in a Non-Cooperative Environment, *J Intell Robot Syst*, 2013 (70): 315-327.

[8] H. S. David, S. Shankar, An Evasive Maneuvering Algorithm for UAVs in See-and-Avoid Situations, in *Proceedings of the 20007 American Control Conference*, 2007: 3886-3891.

[9] B. Antoine, Z. Jean-Christophe, and F. Dario, Vision-based control of near-obstacle flight, *Auton Robot*, 2009 (27): 201–219.

[10] M. Aaron, C. Peter, and M. Luis, Rotorcraft Collision Avoidance using Spherical Image-based Visual Servoing and Single Point Features, in *Proceedings of IEEE/RSJ International Conference on Intelligent Robots and Systems*, 2012: 1199-1205.

[11] M. Aaron, M. Luis, C. Peter, and P. Cédric , Aircraft Collision Avoidance using Spherical Visual Predictive Control and Single Point Features, in *Proceedings of IEEE/RSJ International Conference on Intelligent Robots and Systems*, 2013: 50-56.

[12] N. B. Khristo, Spirals and Conchospirals in the Flight of Insects, *The College Mathematics Journal*, 1999, 30(1): 23-31.

[13] H. H. Wesley, R. F. Brett, R. F. Jonathan, and H. W. William, Visual navigation and obstacle avoidance using a steering potential function, *Robotics and Autonomous Systems*, 2006 (54): 288-299.

[14] B. R. Fajen, W. H. Warren, Behavioral dynamics of steering, obstacle avoidance, and route selection, *Journal of Experimental Psychology: Human Perception and Performance*, 2003, 29 (2): 343–362.

[15] B. R. Fajen, W. H.Warren, S. Termizer, and L. P. Kaebling, A dynamical model of steering, obstacle avoidance, and route selection, *International Journal of Computer Vision*, 2003, 54 (1–2): 13–34.

[16] W. H. Warren, B. R. Fajen, From optic flow to laws of control, in *L.M. Vaina, S.A. Beardsley, S. Rushton (Eds.), Optic Flow and Beyond, Kluwer*, 2004: 307–333.

[17] O. Khatib, Real-time obstacle avoidance for manipulators and mobile robots, *International Journal of Robotics Research*, 1986, 5 (1): 90–98.

[18] R. N. Derek , D. B. Barber, W. M. Timothy and W. B. Randal, Vector Field Path Following for Miniature Air Vehicles, *IEEE Trans. on ROBOTICS*, 2007, 23(3): 519–529.

[19] T. F. Romeo, C. François, Improvements on Visual Servoing From Spherical Targets Using a Spherical Projection Model, *IEEE Trans. on ROBOTICS*, 2009, 25(4): 874-886.

[20] B. Z. Daniel, Q. P. Madeleine, and G. Cole, Dynamic visual cues induce jaw opening and closing by tiger beetles during pursuit of prey, *Biology letters*, 2014 (10): 1-4.